Supplementary Materials for

Electron transfer driving force as the criterion for efficient n-doping of organic semiconductors with DMBI-H derivatives

Chunlin Xu and Dong Wang*

*Laboratory of Flexible Electronics Technology, Tsinghua University, Beijing 100084,
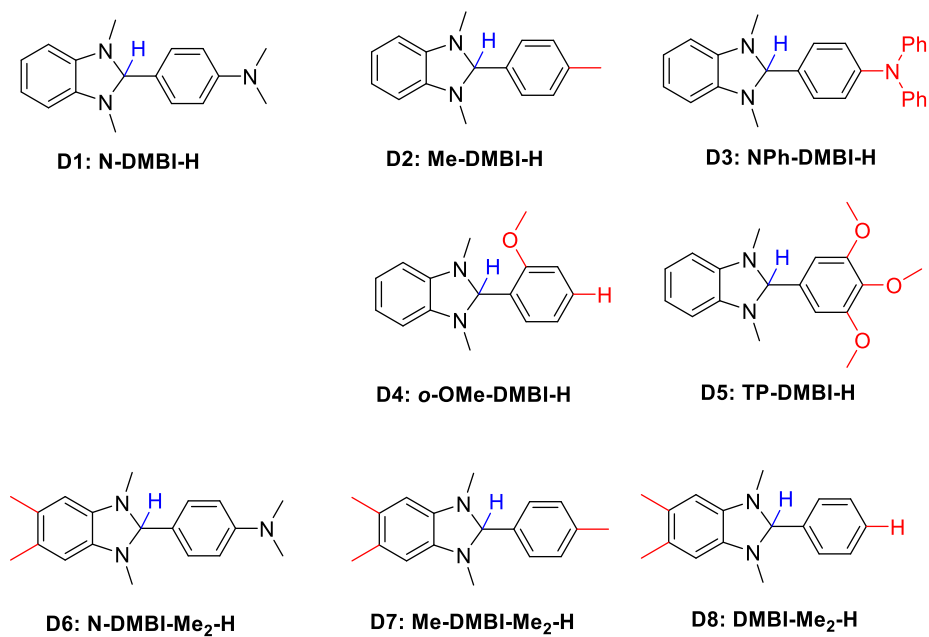People's Republic of China*

*MOE Key Laboratory of Organic OptoElectronics and Molecular Engineering,
Department of Chemistry, Tsinghua University, Beijing 100084, People's Republic of
China*

*Corresponding author. Email: dong913@tsinghua.edu.cn*

Contents

Molecule structures of dopants and OSCs

D1: N-DMBI-H　　　**D2: Me-DMBI-H**　　　**D3: NPh-DMBI-H**

D4: *o*-OMe-DMBI-H　　　**D5: TP-DMBI-H**

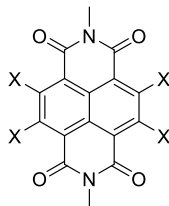**D6: N-DMBI-Me$_2$-H**　　　**D7: Me-DMBI-Me$_2$-H**　　　**D8: DMBI-Me$_2$-H**

Fig. S1. Molecular structures of DMBI-H derivates considered in this work. The active C-H bond is highlighted in blue, and the structure difference from *N*-DMBI-H is highlighted in red.
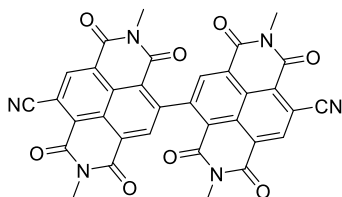
I: Small molecules
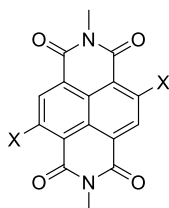
SM1: X=F, 2F-NDI
SM2: X=Cl, 2Cl-NDI
SM3: X=Br, 2Br-NDI
SM4: X=CN, 2CN-NDI
SM5: X=CH_3, 2CH_3-NDI
SM6: X=OCH_3, 2OCH_3-NDI
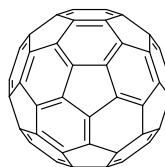SM7: X=NH_2, 2NH_2-NDI

SM8: X=H, NDI
SM9: X=F, 4F-NDI
SM10: X=Cl, 4Cl-NDI
SM11: X=Br, 4Br-NDI
SM12: X=CN, 4CN-NDI
SM13: X=CH_3, 4CH_3-NDI
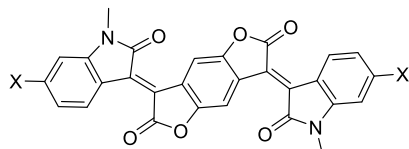SM14: X=OCH_3, 4OCH_3-NDI
SM15: X=NH_2, 4NH_2-NDI

SM16: (CN-NDI)$_2$
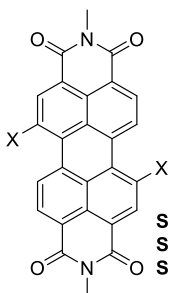
SM17: X=H, PDI
SM18: X=Br, 2Br-PDI
SM19: X=CN, 2CN-PDI

SM20: C60

SM21: X=H, BDOPV
SM22: X=Br, 2Br-BDOPV
SM23: X=CN, 2CN-BDOPV
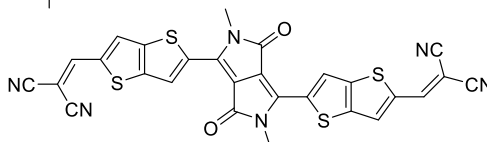
SM24: A-DCV-DPPTT
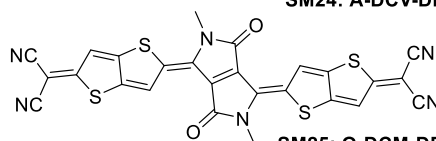
SM25: Q-DCM-DPPTT

II: Polymers

P1: PNDI-T2

n = 1, 2, 3

P2: BBL

n = 1, 2, 3
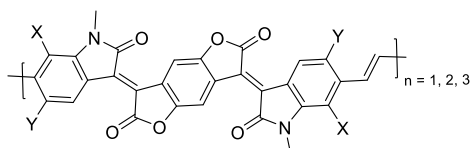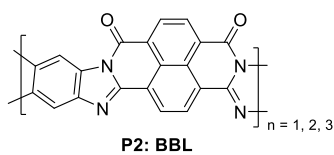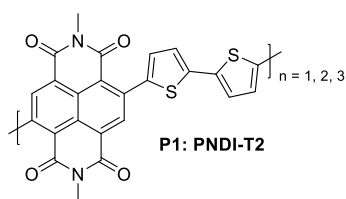
P3: X=Y=H, BDPPV
P4: X=F, Y=H, FBDPPV
P5: X=H, Y=Cl, ClBDPPV

n = 1, 2, 3

P6: TBDPPV

n = 1, 2, 3

P7: TBDPPV-T

n = 1, 2, 3

P9: LPPV

n = 1, 2, 3

P8: TBDPPV-2T

n = 1, 2, 3

P10: BIBI

n = 1, 2, 3

P11: PBTI1

n = 1, 2, 3

P12: PBTI2

n = 1, 2, 3

P13: PBTI3

n = 1, 2, 3

P14: PBTzI

n = 1, 2, 3

P15: PDTzTI

n = 1, 2, 3

P16: X=H, PDTzTIT
P17: X=F, PDTzTIT-2F

n = 1, 2,3

P18: X=H, PDDP[T]$_2$-T
P19: X=F, PDDP[T]$_2$-TF$_2$

n = 1, 2, 3

P20: P(TDPP-CT2)

n = 1, 2, 3

P21: X=H, PDDP[Py]$_2$-T
P22: X=F, PDDP[Py]$_2$-TF$_2$

n = 1, 2, 3

P23: P(PzDPP-CT2)

n = 1, 2, 3

S4
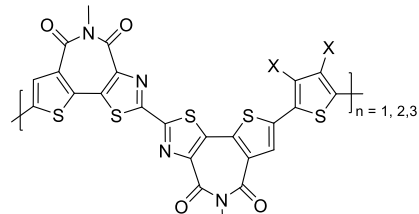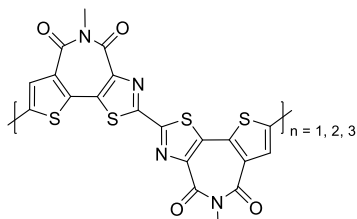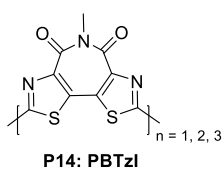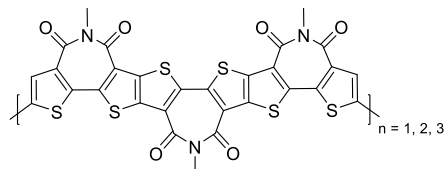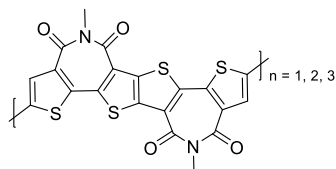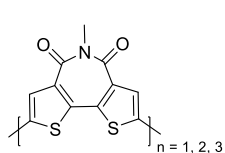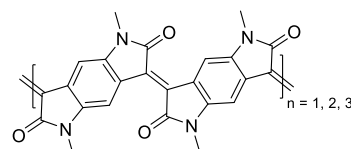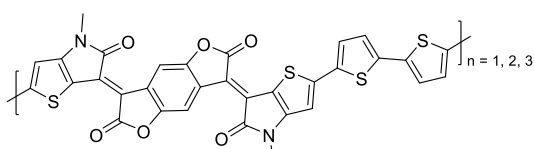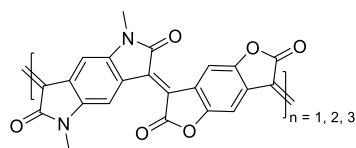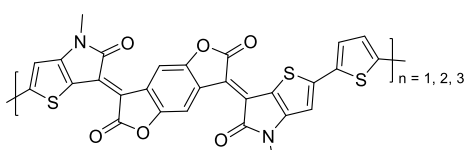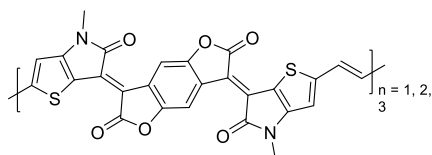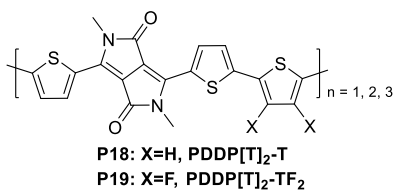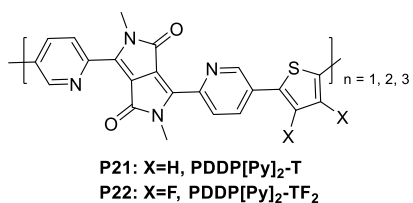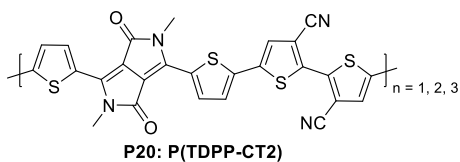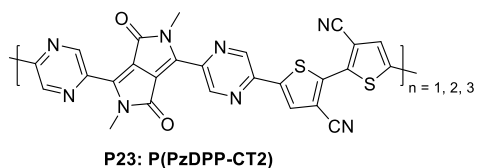
III: Designed polymers
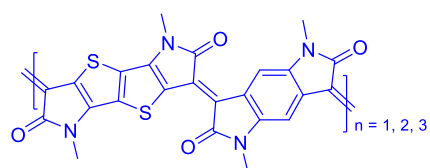
P24: TIBI
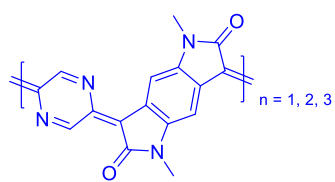
P25: BzBI
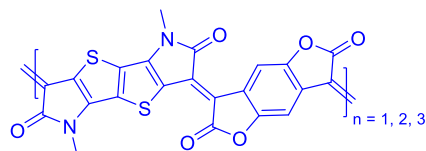
P26: TIBF
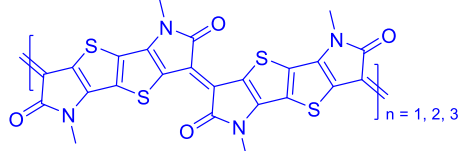
P27: TITI

Fig. S2. Molecular structures of OSCs considered in this work.

Optimal hydrogen atom/hydride adsorption sites
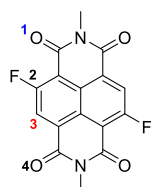
SM1

Site	H⁻	H•
1	2.5	0.0
2	-1.2	17.0
3	0.0	10.6
4	11.2	7.1
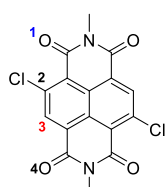
SM2

Site	H⁻	H•
1	0.5	0.0
2	-37.3	8.2
3	0.0	10.7
4	10.1	7.4
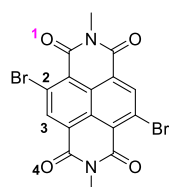
SM3

Site	H⁻	H•
1	0.0	0.0
2	-35.4	3.8
3	0.9	11.8
4	8.9	6.5
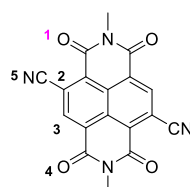
SM4

Site	H⁻	H•
1	0.0	0.0
2	5.4	18.9
3	6.2	13.9
4	8.3	5.4
5	11.3	9.7
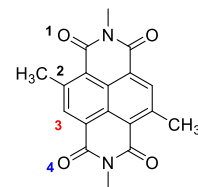
SM5

Site	H⁻	H•
1	8.9	1.1
2	1.2	6.2
3	0.0	3.9
4	7.9	0.0
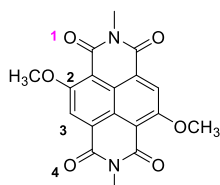
SM6

Site	H⁻	H•
1	0.0	0.0
2	3.3	20.2
3	0.1	11.9
4	13.4	13.8
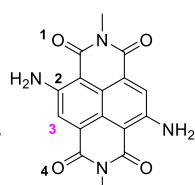
SM7

Site	H⁻	H•
1	14.1	3.2
2	23.4	23.9
3	0.0	0.0
4	27.0	9.1
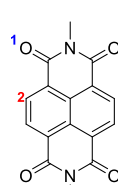
SM8

Site	H⁻	H•
1	7.1	0.0
2	0.0	5.2
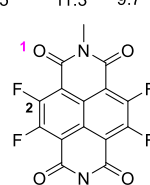
SM9

Site	H⁻	H•
1	0.0	0.0
2	-12.1	11.0
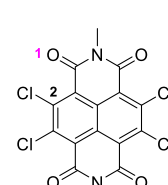
SM10

Site	H⁻	H•
1	0.0	0.0
2	-36.2	2.6
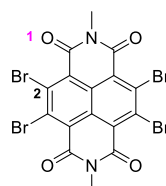
SM11

Site	H⁻	H•
1	0.0	0.2
2	-33.5	0.0
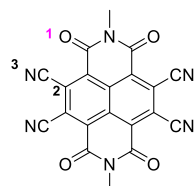
SM12

Site	H⁻	H•
1	0.0	0.0
2	6.3	20.2
3	6.3	9.4
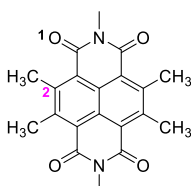
SM13

Site	H⁻	H•
1	16.4	3.4
2	0.0	0.0
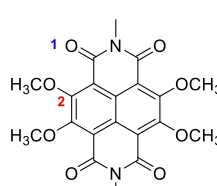
SM14

Site	H⁻	H•
1	4.0	0.0
2	0.0	12.2
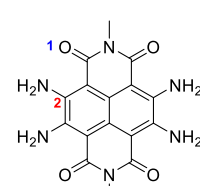
SM15

Site	H⁻	H•
1	5.6	0.0
2	0.0	1.2

SM16
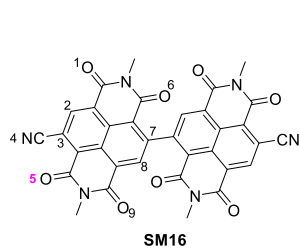
Site	H⁻	H•
1	6.1	1.0
2	5.5	8.8
3	7.4	14.2
4	11.5	6.7
5	0.0	0.0
6	0.1	1.1
7	0.3	9.9
8	4.4	7.3
9	4.7	0.6

SM17
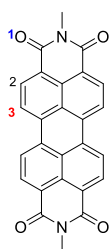
Site	H⁻	H•
1	6.0	0.0
2	8.7	10.2
3	0.0	1.2

SM18
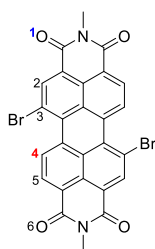
Site	H⁻	H•
1	3.3	0.0
2	5.7	7.6
3	-40.6	-6.9
4	0.0	3.4
5	6.2	9.0
6	5.2	0.6

SM19
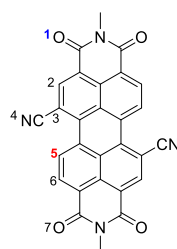
Site	H⁻	H•
1	4.5	0.0
2	11.8	11.3
3	4.1	8.5
4	12.6	9.3
5	0.0	3.9
6	7.5	11.5
7	5.3	0.0

SM20

Site	H⁻	H•
1	0.0	0.0

SM21
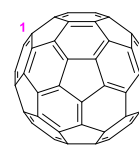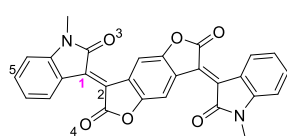
Site	H⁻	H•
1	0.0	0.0
2	17.8	4.1
3	14.8	6.5
4	25.4	7.9

SM22
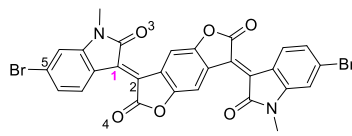
Site	H⁻	H•
1	0.0	0.0
2	16.3	3.9
3	13.8	6.0
4	23.2	6.9
5	-10.2	9.2

SM23
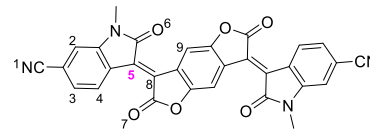
Site	H⁻	H•
1	26.5	17.0
2	31.6	20.2
3	31.4	18.0
4	14.8	13.4
5	0.0	0.0
6	6.8	1.4
7	19.4	5.8
8	13.2	4.3
9	20.2	12.0

SM24
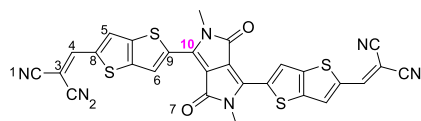
Site	H⁻	H•
1	16.4	11.5
2	15.3	11.5
3	6.0	5.8
4	0.7	7.2
5	8.1	6.0
6	4.3	2.3
7	10.5	4.8
8	10.4	8.8
9	15.8	10.6
10	0.0	0.0

SM25
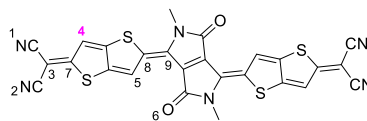
Site	H⁻	H•
1	9.4	6.9
2	8.5	6.1
3	1.4	0.8
4	0.0	0.0
5	11.5	11.4
6	8.8	8.2
7	1.8	25.1
8	5.8	8.8
9	10.2	7.9
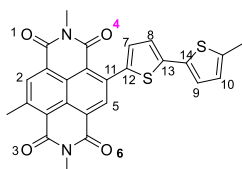
P1

Site	H⁻	H•
1	9.6	8.0
2	2.2	12.2
3	11.0	9.2
4	0.0	0.0
5	2.9	11.1
6	8.5	7.5
7	4.1	9.4
8	23.0	10.9
9	6.2	6.3
10	40.6	22.0
11	2.4	14.0
12	16.1	3.6
13	4.8	8.1
14	32.4	14.4
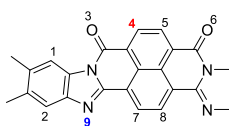
P2

Site	H⁻	H•
1	37.7	24.0
2	17.4	18.6
3	10.5	13.2
4	0.0	15.7
5	7.9	17.3
6	11.8	14.4
7	2.2	14.4
8	9.3	16.6
9	4.1	0.0
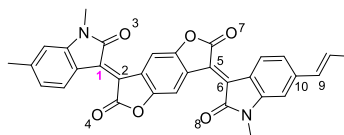
P3

Site	H⁻	H•
1	0.0	0.0
2	18.2	4.0
3	15.1	7.3
4	25.9	8.4
5	16.6	2.9
6	0.8	1.2
7	24.6	7.7
8	10.6	7.5
9	22.1	19.4
10	21.6	19.6
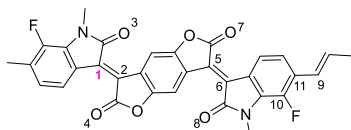
P4

Site	H⁻	H•
1	0.0	0.0
2	17.5	4.4
3	14.2	6.3
4	24.7	8.0
5	15.8	3.1
6	0.9	1.3
7	23.3	7.3
8	9.6	6.6
9	20.5	19.7
10	41.1	24.1
11	42.0	22.7
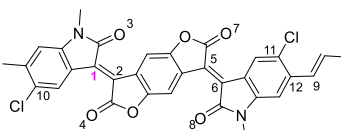
P5

Site	H⁻	H•
1	0.0	0.0
2	17.0	4.4
3	9.6	6.3
4	23.8	7.4
5	15.4	3.7
6	0.7	0.8
7	22.6	7.1
8	9.9	6.6
9	21.0	16.3
10	36.4	10.3
11	31.6	5.8
12	15.2	13.5
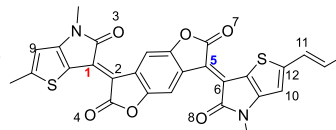
P6

Site	H⁻	H•
1	0.0	4.6
2	15.1	1.7
3	7.5	5.9
4	23.1	7.2
5	12.8	0.0
6	0.9	5.8
7	17.8	6.4
8	7.5	8.5
9	37.2	25.1
10	32.4	17.1
11	45.8	19.2
12	0.0	1.9
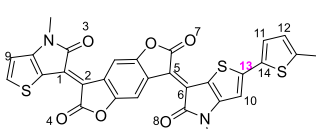
P7

Site	H⁻	H•
1	1.7	4.8
2	16.9	2.1
3	15.3	6.3
4	24.8	8.2
5	13.9	0.6
6	3.0	6.7
7	19.1	7.2
8	9.3	9.8
9	39.3	25.4
10	32.7	16.2
11	3.1	2.0
12	49.5	24.8
13	0.0	0.0
14	23.9	17.4
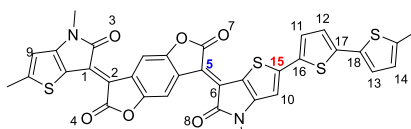
P8

Site	H⁻	H•
1	1.0	4.3
2	18.5	1.9
3	8.3	6.0
4	23.9	7.9
5	11.3	0.0
6	2.7	6.6
7	16.8	6.6
8	14.9	9.5
9	37.9	25.1
10	29.4	14.1
11	4.4	3.7
12	35.8	14.5
13	7.2	4.6
14	49.9	23.9
15	0.0	0.3
16	30.8	12.4
17	4.7	3.8
18	38.1	16.0
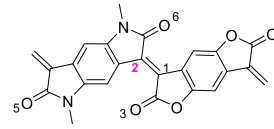
P9

Site	H⁻	H•
1	7.3	0.2
2	0.0	0.0
3	18.0	6.0
4	43.1	18.5
5	36.6	14.9
6	8.4	5.1
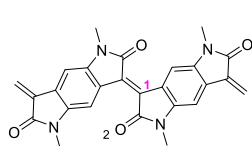
P10

Site	H⁻	H˙
1	0.0	0.0
2	8.3	8.4
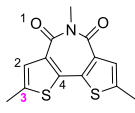
P11

Site	H⁻	H˙
1	25.5	13.2
2	34.2	13.4
3	0.0	0.0
4	1.9	4.7
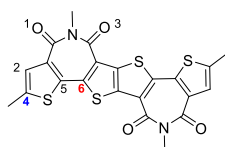
P12

Site	H⁻	H˙
1	24.7	12.0
2	35.5	14.9
3	37.6	15.0
4	1.6	0.0
5	12.8	6.7
6	0.0	3.3
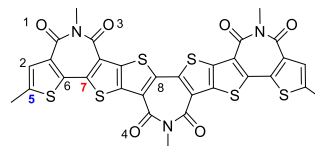
P13

Site	H⁻	H˙
1	23.1	11.1
2	33.6	17.0
3	37.2	15.4
4	26.1	13.0
5	2.3	0.0
6	16.7	7.0
7	0.0	3.2
8	3.8	4.2
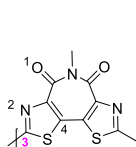
P14

Site	H⁻	H˙
1	24.7	7.0
2	28.0	0.5
3	0.0	0.0
4	4.1	2.7
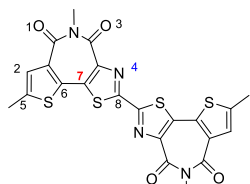
P15

Site	H⁻	H˙
1	23.1	13.7
2	21.9	7.3
3	38.5	19.7
4	9.5	0.0
5	2.7	4.5
6	13.6	9.2
7	0.0	9.3
8	9.3	12.6
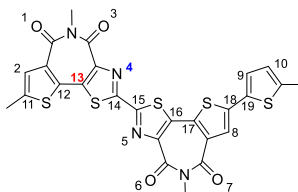
P16

Site	H⁻	H˙
1	22.6	14.0
2	32.3	16.3
3	38.2	20.1
4	7.9	0.0
5	8.8	0.3
6	19.4	6.4
7	22.2	14.3
8	26.2	10.3
9	7.2	5.8
10	44.7	21.4
11	2.8	4.8
12	14.1	9.6
13	0.0	9.5
14	9.7	13.0
15		11.5
16	0.1	10.1
17	9.1	6.0
18	6.4	9.2
19	35.6	13.3
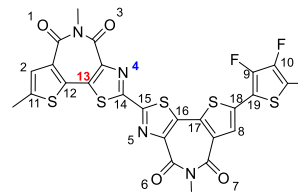
P17

Site	H⁻	H˙
1	22.4	14.1
2	32.1	16.5
3	38.1	20.4
4	7.3	0.0
5	8.7	0.6
6	19.0	6.4
7	22.6	14.8
8	24.8	10.4
9	1.1	5.9
10	-9.8	15.9
11	2.8	5.1
12	14.3	9.8
13	0.0	9.8
14	10.0	13.2
15	6.9	12.1
16	0.0	10.2
17	8.4	7.0
18	5.9	9.8
19	35.8	15.0
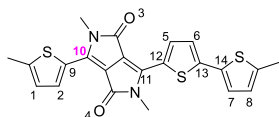
P18

Site	H⁻	H˙
1	48.7	24.8
2	3.2	2.8
3	23.8	10.6
4	26.6	11.4
5	6.5	5.0
6	37.8	14.7
7	4.6	4.4
8	47.4	22.8
9	26.7	18.0
10	0.0	0.0
11	3.4	1.1
12	31.3	13.0
13	2.6	2.9
14	36.1	14.9
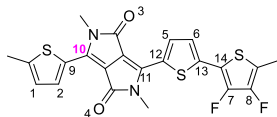
P19

Site	H⁻	H˙
1	55.5	24.7
2	3.6	2.7
3	29.1	13.3
4	26.5	10.8
5	8.7	5.5
6	36.1	14.4
7	-2.2	2.9
8	-13.2	16.3
9	26.8	17.9
10	0.0	0.0
11	4.0	0.9
12	30.7	13.0
13	2.8	2.9
14	33.8	15.7
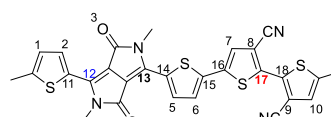
P20

Site	H⁻	H˙
1	53.0	24.9
2	5.5	2.5
3	25.8	9.6
4	19.2	8.5
5	13.7	4.9
6	20.1	11.6
7	10.6	5.8
8	22.8	15.6
9	10.3	11.6
10	39.0	21.4
11	27.7	18.2
12	1.4	0.0
13	8.7	0.1
14	19.5	10.8
15	9.0	2.3
16	18.6	11.9
17	0.0	1.2
18	18.8	7.6

P21

Site	H⁻	H·
1	40.0	33.9
2	41.4	34.0
3	6.6	0.0
4	23.2	27.2
5	11.3	3.0
6	14.4	3.7
7	5.8	0.1
8	24.5	28.5
9	30.0	29.5
10	33.9	30.6
11	20.5	21.5
12	58.6	34.3
13	50.8	38.5
14	0.0	5.3
15	2.4	5.9
16	35.5	31.5
17	24.8	30.7
18	46.5	25.9

P22

Site	H⁻	H·
1	40.8	34.2
2	42.0	34.3
3	6.4	0.0
4	23.2	27.4
5	10.5	19.1
6	14.1	3.7
7	5.9	0.6
8	24.8	28.5
9	30.2	30.5
10	32.4	30.7
11	11.8	20.3
12	0.1	29.1
13	51.6	38.9
14	0.0	5.8
15	3.4	6.4
16	37.5	33.8
17	25.8	31.6
18	45.4	26.4

P23

Site	H⁻	H·
1	16.4	2.0
2	31.5	23.1
3	9.6	1.5
4	11.6	14.4
5	24.0	7.7
6	16.0	7.2
7	9.9	1.6
8	13.9	16.6
9	10.5	2.0
10	20.9	19.9
11	11.6	11.6
12	28.0	19.0
13	12.6	15.1
14	40.7	24.5
15	46.9	31.1
16	0.0	0.0
17	6.4	1.3
18	25.4	25.1
19	15.1	19.1
20	23.5	14.1
21	1.6	6.3
22	24.4	10.4

P24

Site	H⁻	H·
1	0.0	0.0
2	4.9	10.2
3	8.8	9.9
4	33.4	19.3
5	37.5	22.0
6	9.3	10.7

P25

Site	H⁻	H·
1	0.0	0.0
2	0.0	15.5
3	8.5	7.1
4	33.0	23.3

P26

Site	H⁻	H·
1	3.6	0.0
2	0.0	9.3
3	10.7	7.0
4	35.2	18.6
5	30.3	15.4
6	35.2	18.6

P27

Site	H⁻	H·
1	0.0	0.0
2	10.9	6.0
3	27.4	13.0

Fig. S3. Possible adsorption sites of the hydride (H⁻) and hydrogen atom (H·) and the relative energies in kcal/mol at (U)B3LYP/6-31G** level in CHCl₃. The optimal adsorption sites are highlighted: red for hydride, blue for the hydrogen atom, and pink for both of them. Some sites with adsorption energies lower than the optimal sites are excluded (highlighted in orange) because optimized structures show that the carbon-halogen bonds are broken by the adsorption of a hydride or hydrogen atom to these sites. The zero-point energy (ZPE) correction of vibration is not included here to save the computational cost.
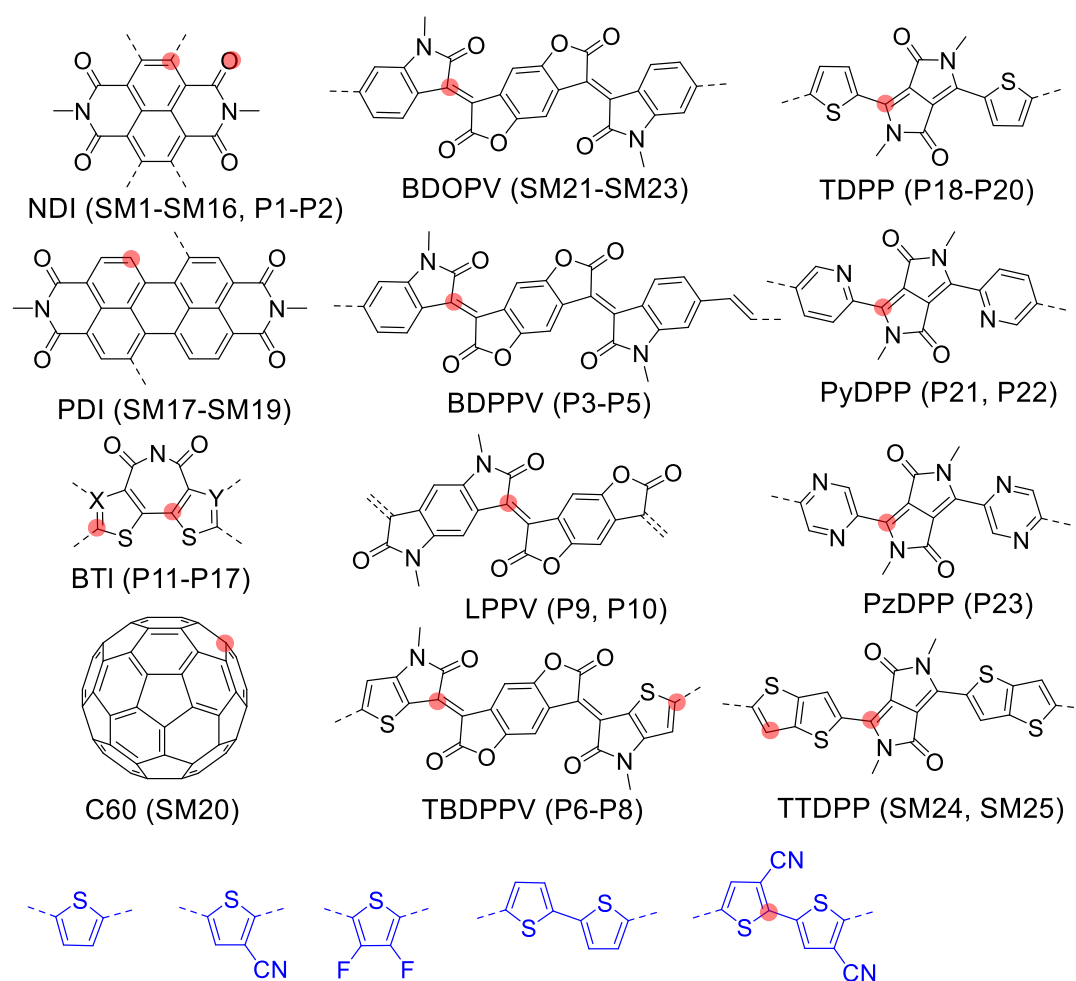
Fig. S4. The structures of the electron-withdrawing (black) and electron-donating (blue) moieties of considered OSCs, the possible optimal hydride addition sites are highlighted in red. They are grouped into 12 categories: Naphthalene diimide (NDI), perylene diimide (PDI), C60, benzodifurandione-based oligo(*p*-phenylene vinylene) (BDOPV), benzodifurandione-based poly(*p*-phenylenevinylene) (BDPPV), thiophene-fused benzodifurandione-based poly(*p*-phenylenevinylene) (TBDPPV), bis-isatin-based benzodifurandione-based poly(*p*-phenylenevinylene) (LPPV), bithiophene imide (BTI), thiophene-flanked diketopyrrolopyrrole (TDPP), pyridine-flanked diketopyrrolopyrrole (PyDPP), pyrazine-flanked diketopyrrolopyrrole (PzDPP), as well as thiophthene-flanked diketopyrrolopyrrole (TTDPP).
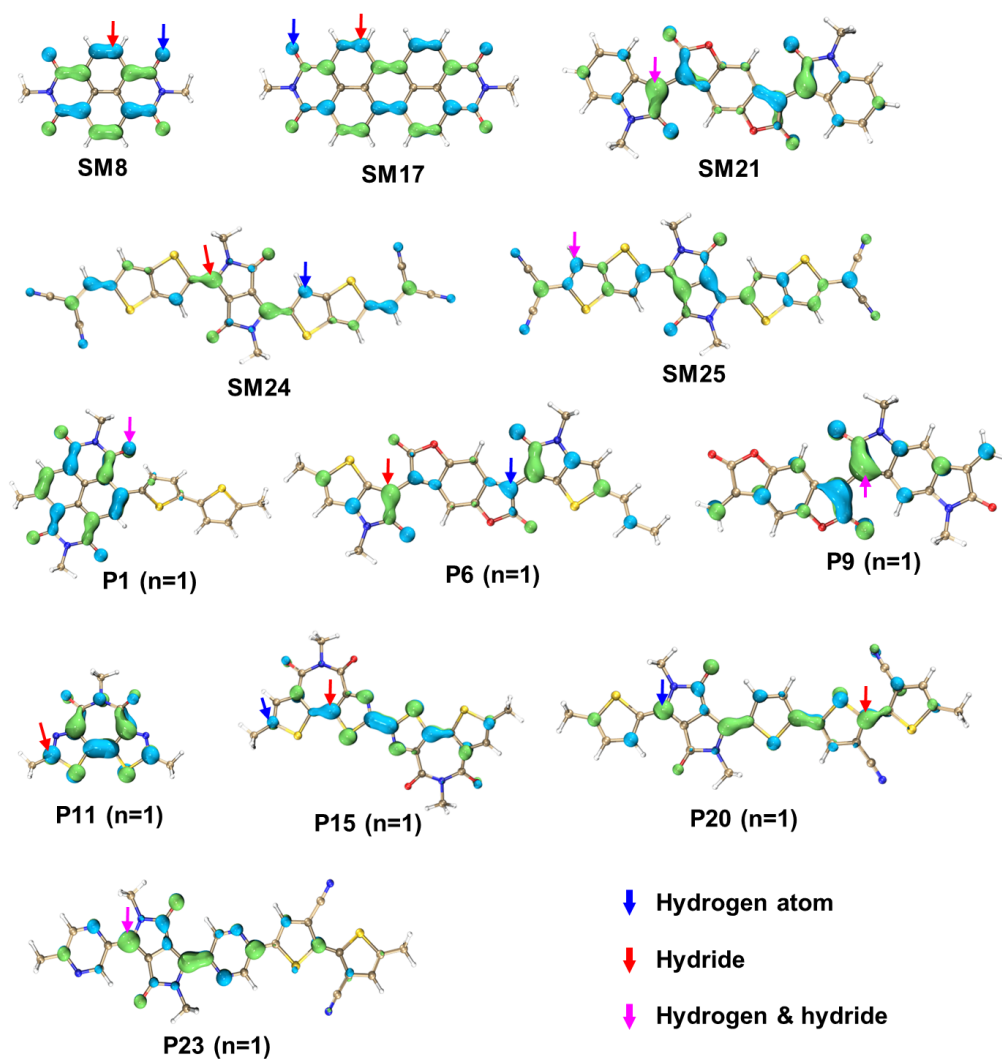
Fig. S5. The LUMO (iso = 0.05) of representative small molecules and polymers (n = 1). The optimal addition sites of hydrogen atom (in blue), hydride anion (in red), and both of them (in purple) are marked by arrows.

Additional discussions about HYT

The Gibbs free energy of activation, $\Delta G^{\ddagger}$ of HYT from N-DMBI-H to OSCs was calculated by optimizing the structure of transition state (TS) where the transferring species [H] (may it be $H^{\bullet}$, H^{+}, or H^{-}) is located between the donor carbon atom of N-DMBI-H and the acceptor atom of OSCs. 2CN-BDOPV, Q-DCV-DPPTT, NDI-T2, and C60 are chosen as representative OSCs for their typical chemical structures (Fig. S6a). To show the amount of electron transfer (Q_{ET}) from N-DMBI-H to OSCs during the reaction, the natural population analysis[1] is performed along the intrinsic reaction coordinate. The charges on the [D], [H], and [A] species, respectively, are shown in S6b, with $Q_D + Q_H + Q_A = 0$ for the whole reaction complex. On the reactant side, the Q_{ET} can be estimated by the charge on [A] (Q_A). For NDI-T2 (EA = 3.7 eV) and C60 (EA = 3.8 eV) with small EAs, there is only 0.25e transferred from N-DMBI-H (IE = 5.1 eV) to OSCs. But there is a notable Q_{ET} around 0.5e for 2CN-BDOPV and Q-DCM-DPPTT with relatively large EAs (4.3 eV and 4.7 eV, respectively). On the product side, the Q_{ET} can be estimated by the charge on [D] (Q_D), $Q_D \approx +1e$ for all the OSCs indicates that an integrated electron has been transferred from DH to A, accompanying the [H] transfer. Notably, the charge on the [H] species (Q_H) is much less than +1e and remains constant during the reaction for all cases except for NDI-T2. In NDI-T2, Q_H increases from +0.25e on the reactant side to +0.5e on the product side, which can be attributed to the electronegativity difference between the donor carbon and the acceptor oxygen atom which is the optimal [H]-addition site of NDI-T2. This shows that the transferring [H] species is $H^{\bullet}$ rather than H^{-} or proton. These results strongly support the HYT mechanism that describes the transfer of one hydrogen atom and one electron, and the electron transfer starts with the hydrogen atom transfer. As the r_{D-H} increases, $H^{\bullet}$ moves from D to A, and the amount of electron transfer increases, which is concordant with the HYT *via* concerted electron and hydrogen atom transfer.

The Distortion/Interaction analysis[2] is performed to further understand the formation of TS. The total energy change (ΔE_{tot}) along the IRC is divided into the

distortion energy (ΔE_d) and the interaction energy (ΔE_{inter}), and $\Delta E_{tot} = \Delta E_d + \Delta E_{inter}$. ΔE_d is the energy difference caused by the geometry distortion of reactants, DH and A along the IRC, whose value is positive, and ΔE_{inter} refers to the intermolecular interaction between reactants, whose value is negative.[2] Because the dopant is N-DMBI-H for all the OSCs, the difference between ΔE_ds, namely, $\Delta\Delta E_d$ arises predominantly from the structural distortion of OSCs, and it is less than 10 kcal/mol from Fig. S6c. While the maximum $\Delta\Delta E_{inter}$ is up to 30 kcal/mol, governing the $\Delta\Delta E_{tot}$. On the reactant side, the trend of ΔE_{inter} is consistent with Q_{ET}: for 2CN-BDOPV and Q-DCM-DPPTT with larger EAs and Q_{ET}s, the ΔE_{inter}s are more negative than NDI-T2 and C60 which have smaller EAs and Q_{ET}s. Hence, the ΔE_{inter} is dictated by the Coulomb attraction caused by the ET. As a result, the trend of $\Delta G^{\ddagger}$ is in line with the EA of OSCs, because large EA can promote ET, enhance ΔE_{inter} and eventually lowers $\Delta G^{\ddagger}$. The polarization, dispersion, and induction interactions may also take a role in ΔE_{inter}, making the trend of ΔE_{inter} deviate from that of Q_{ET}. For example, the π-π interaction in the N-DMBI-H/Q-DCM-DPPTT system is weaker than the N-DMBI-H/2CN-BDOPV complex due to the smaller contact area between N-DMBI-H and OSC in the former (see Fig. S7). In N-DMBI-H/2CN-BDOPV, there is an evident π-π interaction (in green) between the (dimethylamino)phenyl of N-DMBI-H and 2CN-BDOPV, while it does not exist in N-DMBI-H/Q-DCM-DPPTT. As a result, the ΔE_{inter} of the former is slightly less negative than the latter, which is opposite to the trend of Q_{ET}.

To depict the HYT process, the localized molecular orbitals (LMOs) analysis of N-DMBI-H/2CN-BDOPV in its TS is illustrated in Fig. S8. We divide the activated complex DHA‡ into DH‡ and A‡, and analyze the interactions between them with LMOs. When the C-H bond is elongated and the bonding orbital of the dopant (labeled as $\sigma_{DH^{\ddagger}(C\text{-}H)}$) approaches the empty π^{*} orbital of the OSC that is mainly composed of the p_z orbital on the hydride adsorption atom (labeled as $\pi^{*}_{A^{\ddagger}(p_z)}$), they interact to form two three-center σ-type bonds named as $\sigma_{DHA^{\ddagger}}$ and $\sigma^{*}_{DHA^{\ddagger}}$. The bonding orbital $\sigma_{DHA^{\ddagger}}$

is filled and the antibonding orbital $\sigma^*_{DHA^\ddagger}$ has a node on the transferring $H^\bullet$, which is the character of HAT,[3, 4] and it is unoccupied. Meanwhile, as the C-H bond of the dopant is stretched, the energy of $\pi_{DH^\ddagger}$s also increases (the upper limit is $E_{SOMO}(D^\bullet)$), and the $\pi - \pi$ overlap near the reaction center can assist the ET from $\pi_{DH^\ddagger}$s to $\pi_{A^\ddagger}$s at the time of HAT. The larger EA (the smaller IE) of A ($D^\bullet$) will cause promoted ET that enhances the Coulomb interaction and reduces the activation energy, which eventually facilitates the HYT. The conclusion of LMOs analysis is in line with that of Distortion/Interaction energy analysis[2] (see Figs. S6c). The $\Delta G^\ddagger$s of 2CN-BDOPV (7.8 kcal/mol) and Q-DCM-DPPTT (11.2 kcal/mol) with larger EAs are significantly lower than NDI-T2 (27.3 kcal/mol) and C60 (20.2 kcal/mol) with smaller EAs. It should be noted that there exist several $\pi_{DH^\ddagger}$s and $\pi^*_{A^\ddagger}$s that contribute to the ET in the LMOs basis, for brevity, Fig. S8 only shows those with the largest contribution.
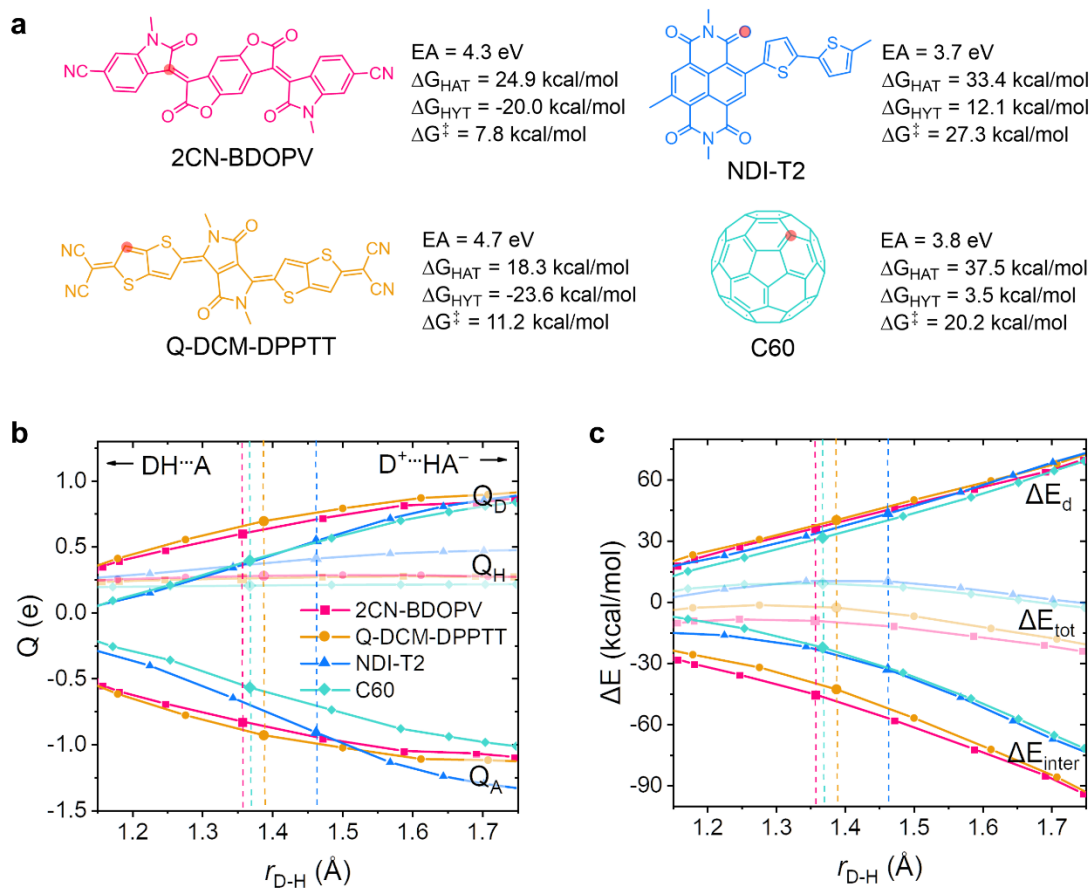
Fig. S6. (a) Molecular structures of representative OSCs with EAs, ΔGs, and $\Delta G^{\ddagger}$s. The optimal [H]-addition sites are highlighted in red. (b) Charges on the [D] and [A] species (Q_D and Q_A), as well as that on the transferring [H] (Q_H) along the IRC (plotted as the C-H bond length of the dopant, r_{D-H}). (c) Changes of the distortion energy (ΔE_d), interaction energy (ΔE_{inter}), and total energy (ΔE_{tot}) along the IRC. The vertical dashed lines indicate the position of transition states.
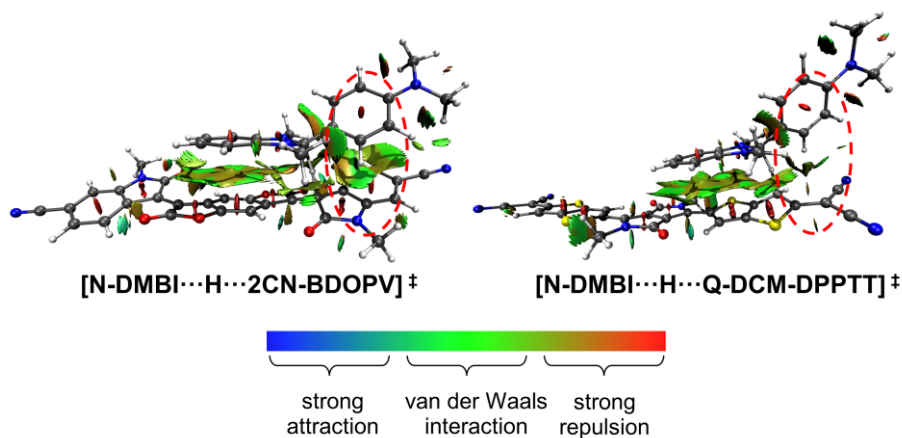
Fig. S7. The noncovalent interacting (NCI)[5] maps of the *N*-DMBI-H/2CN-BDOPV and the *N*-DMBI-H/Q-DCM-DPPTT systems in the TS obtained using Multiwfn code.[6]
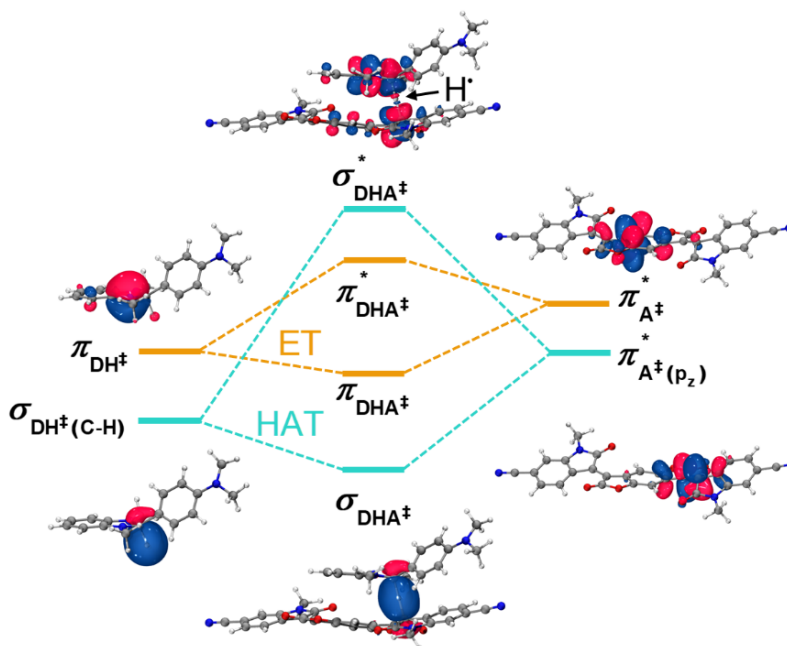
Fig. S8. Schematic diagrams of the concerted ET and HAT mechanism based on the LMOs of dopant (DH‡), OSC (A‡), and the activated complex (DHA‡) in the TS.

Criterion for efficient n-doping
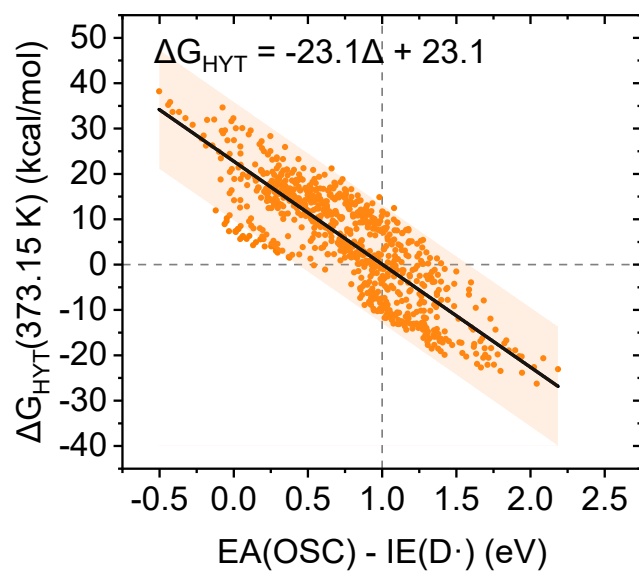
Fig. S9. The ΔG_{HYT} at 373.15 K as a function of EA(OSC) -IE(D$^{\cdot}$).
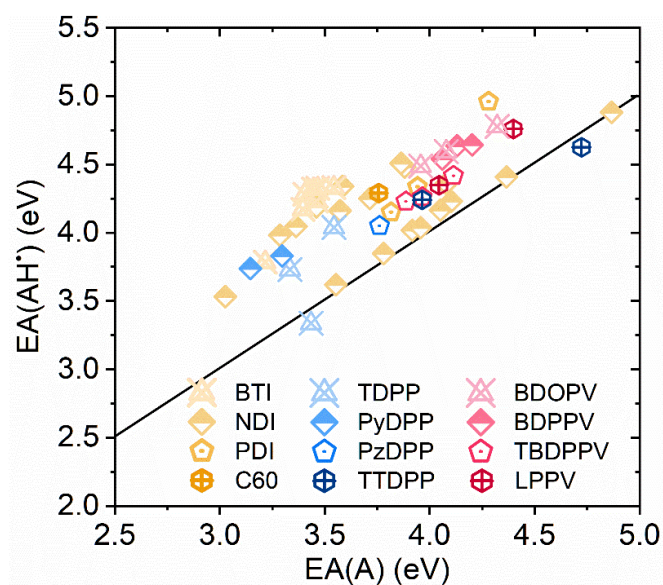
Fig. S10. EA(A) *vs*. EA(AH$^{\bullet}$) of considered OSCs which are highlighted as per the classification of backbone structures, see Fig. S4.
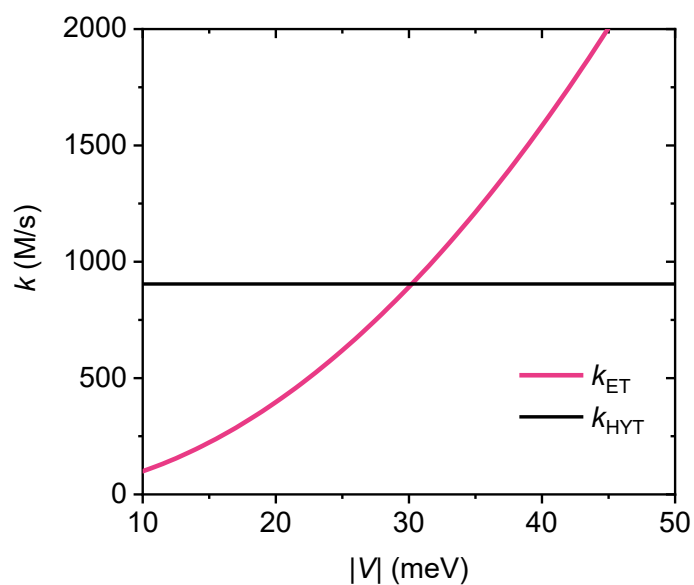
Fig. S11. Rate constants (298.15 K) of HYT (k_{HYT}) and ET (k_{ET}) in the doping reaction between BDPPV and *N*-DMBI-H. The k_{HYT} was calculated with Eq. (6), and the k_{ET} which changes with the electronic coupling ($|V|$) was calculated using the Marcus equation.[7] Since $|V|$ is sensitive to the molecular packing structure, and the hydride addition to BDPPV destructs the planar structure and conjugation of AH^{-}, $|V|$ could be diminished. If $|V| < 30$ meV, $k_{ET} < k_{HYT}$, the ET process is the RDS of the doping reaction.
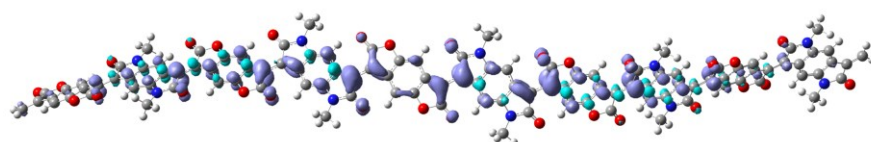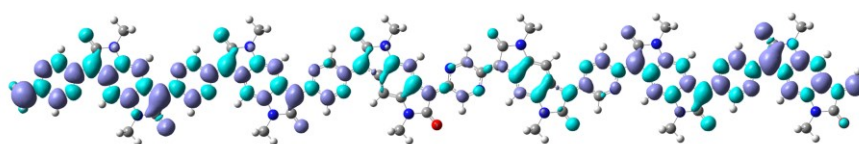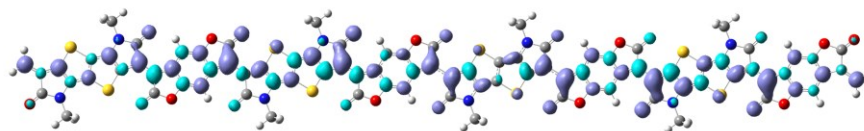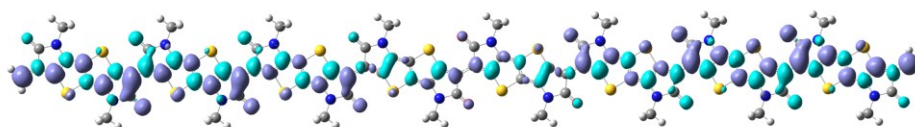
Fig. S12. Spin density plots (iso = 0.001 a.u.$^{-3}$) of oligomer anions of LPPV and designed polymers.

Supplementary data

Table S1. Calculated electron affinities (EA) versus experimental results in eV. The calculation was based on the (U)M06-2X/6-311+G**// (U)B3LYP/6-31G** level in CHCl₃. Note that there is likely some uncertainly in the experimental results based on CV due to different offset values used (4.8 eV or 5.1 eV).

	EA(calc.)	EA(expt.)	method	Ref.
SM1	3.86	3.90	CV	[8]
SM4	4.37	4.50	CV	[8]
SM8	3.71	3.70	CV	[8]
SM17	3.82	3.90		[9]
SM19	4.28	4.30		[9]
SM20	3.76	3.70	IPES	[10]
SM21	3.96	3.96	CV	[11]
SM22	4.08	4.24	CV	[12]
P1	3.78	4.05	IPES	[13]
P2	3.86	4.00		[14]
P3	3.96	4.01, 4.10	CV	[15, 16]
P4	4.20	4.30, 4.17	CV	[16, 17]
P5	4.13	4.30	CV	[17]
P6	4.11	3.95	CV	[18]
P7	3.96	3.86	CV	[18]
P8	3.89	3.81	CV	[18]
P9	4.40	4.49	CV	[19]
P10	4.04	4.40	EA = IP−E$_{opt}$ IP measured by PESA	[20]
P11	3.22	3.45, 3.48	CV	[21, 22]
P12	3.40	3.53	CV	[22]
P13	3.46	3.59	CV	[22]
P14	3.54	3.94	CV	[23]
P15	3.47	3.77	CV	[23]
P16	3.40	3.68	CV	[23]
P17	3.45	3.71	CV	[23]
P18	3.33	3.69	CV	[24]
P19	3.43	3.70	CV	[24]
P20	3.54	3.70	CV	[25]
P21	3.15	3.78	CV	[24]
P22	3.43	3.81	CV	[24]
P23	3.76	4.03	CV	[25]

Table S2. The ionization energy (IE) of dopants (DH) and dopant radicals (D·) in eV as well as the thermodynamic parameters of C-H bond homolysis and heterolysis in kcal/mol at the (U)M06-2X/6-311+G**// B3LYP/6-31G** level in CHCl₃.

	IE (DH)	IE (D·)	ΔG_{homo} (298.15 K)	ΔG_{hetero} (298.15 K)	ΔG_{homo} (373.15 K)	ΔG_{hetero} (373.15 K)
D1	5.05	2.78	71.6	64.8	69.3	63.3
D2	5.15	3.03	69.7	69.1	67.5	67.3
D3	5.13	3.04	68.6	68.0	66.9	66.6
D4	5.08	2.97	69.3	66.9	67.1	65.1
D5	5.18	3.10	70.1	71.3	68.0	69.6
D6	4.87	2.68	71.5	62.4	69.2	60.9
D7	4.95	2.93	69.2	65.7	66.9	63.7
D8	4.98	3.01	68.3	66.6	66.1	65.1

Table S3. The EA in eV, BDE(AH⁻) of OSCs and thermodynamic parameters at 298.15 K in kcal/mol of HYT, ET and the overall doping reaction between N-DMBI-H and OSCs at (U)M06-2X/6-311+G**// B3LYP/6-31G** level in CHCl$_3$.

OSC	EA	BDE(AH⁻)	ΔG_{HYT}	ΔG_{ET}	ΔG_{H2}
SM1	3.86	48.7	6.3	13.8	0.5
SM2	3.88	47.1	6.9	13.3	0.4
SM3	3.92	46.3	6.5	2.0	-1.8
SM4	4.37	48.4	-5.6	-0.8	-13.1
SM5	3.57	46.4	14.8	12.5	6.6
SM6	3.55	50.3	11.9	1.0	7.6
SM7	3.29	55.4	13.5	15.6	14.4
SM8	3.71	44.3	13.5	11.4	3.0
SM9	3.96	45.4	7.6	1.1	-2.4
SM10	4.05	48.0	3.4	2.3	-3.8
SM11	4.10	48.9	1.1	3.2	-4.7
SM12	4.87	51.9	-20.7	0.5	-23.1
SM13	3.36	51.9	14.1	15.4	12.2
SM14	3.58	52.6	9.6	16.8	7.1
SM15	3.03	45.2	28.3	10.7	18.8
SM16	4.08	49.2	1.7	5.6	-4.3
SM17	3.82	46.5	8.8	6.2	0.5
SM18	3.94	45.0	7.6	8.3	-1.7
SM19	4.28	47.5	-2.3	15.0	-9.5
SM20	3.76	53.2	3.5	9.0	-0.5
SM21	3.96	64.6	-12.4	12.0	-1.5
SM22	4.08	64.2	-14.6	11.4	-4.4
SM23	4.32	63.6	-20.0	9.5	-10.9
SM24	3.96	57.1	-6.2	6.3	-2.7
SM25	4.72	57.3	-23.6	-3.2	-20.7
P1 (n=1)	3.68	47.8	12.1	1.4	4.6
P1 (n=2)	3.76	44.8	13.8	-0.9	3.4
P1 (n=3)	3.78	47.7	10.6	1.3	3.4
P2 (n=1)	3.46	49.3	14.1	15.9	8.9
P2 (n=2)	3.78	44.9	11.1	11.6	1.6
P2 (n=3)	3.86	45.1	9.4	11.4	-0.3
P3 (n=1)	3.89	64.5	-11.2	11.8	-0.7
P3 (n=2)	3.95	64.5	-12.1	11.4	-2.2
P3 (n=3)	4.06	63.1	-13.4	11.4	-3.6
P4 (n=1)	4.03	64.4	-14.0	11.2	-3.6
P4 (n=2)	4.09	64.7	-15.4	11.4	-5.1
P4 (n=3)	4.20	62.8	-15.5	9.7	-7.0
P5 (n=1)	4.04	64.1	-14.0	11.9	-3.6
P5 (n=2)	4.05	64.8	-13.7	12.3	-3.4
P5 (n=3)	4.13	63.5	-15.1	12.2	-5.2
P6 (n=1)	3.74	56.2	1.2	9.7	1.8
P6 (n=2)	4.06	51.9	-2.0	5.3	-5.0
P6 (n=3)	4.11	52.3	-4.1	8.1	-5.4

Table S3 Continued

OSC	EA	BDE(AH$^-$)	ΔG_{HYT}	ΔG_{ET}	ΔG_{H2}
P7 (n=1)	3.76	56.0	1.6	7.1	1.9
P7 (n=2)	3.91	54.8	-1.8	7.0	-1.0
P7 (n=3)	3.96	55.0	-2.9	5.4	-3.2
P8 (n=1)	3.77	55.9	1.4	6.9	2.3
P8 (n=2)	3.82	56.2	-0.2	8.3	1.2
P8 (n=3)	3.89	55.8	0.1	5.1	-1.8
P9 (n=1)	3.91	61.7	-8.6	10.3	-0.8
P9 (n=2)	4.31	61.8	-17.8	7.9	-10.8
P9 (n=3)	4.40	60.7	-18.7	8.8	-11.4
P10 (n=1)	3.64	59.0	0.4	5.3	4.5
P10 (n=2)	3.96	61.7	-9.4	8.9	-1.0
P10 (n=3)	4.04	59.9	-7.6	6.5	-3.2
P11 (n=1)	2.60	52.6	31.2	16.2	28.8
P11 (n=2)	2.97	51.9	24.7	14.8	22.0
P11 (n=3)	3.22	47.8	22.4	10.1	13.8
P12 (n=1)	3.02	58.2	16.8	21.1	20.0
P12 (n=2)	3.30	54.8	13.4	18.9	14.6
P12 (n=3)	3.40	54.8	12.3	18.1	12.6
P13 (n=1)	3.29	55.7	13.3	19.0	13.9
P13 (n=2)	3.41	53.7	11.8	16.9	11.4
P13 (n=3)	3.46	54.5	13.0	17.2	11.4
P14 (n=1)	2.83	55.5	23.7	22.6	24.5
P14 (n=2)	3.33	50.7	17.0	17.0	12.7
P14 (n=3)	3.54	49.1	12.9	17.1	7.4
P15 (n=3)	3.20	57.3	12.4	22.2	15.7
P15 (n=1)	3.41	53.4	12.5	18.7	11.4
P15 (n=2)	3.47	54.7	9.0	19.4	9.2
P16 (n=3)	3.26	56.3	11.9	21.7	14.5
P16 (n=1)	3.33	54.8	13.0	19.6	12.6
P16 (n=2)	3.40	55.2	11.4	21.2	12.4
P17 (n=3)	3.29	55.6	13.3	20.7	13.9
P17 (n=1)	3.38	54.2	12.6	19.3	12.0
P17 (n=2)	3.45	55.1	9.0	21.7	10.8
P18 (n=1)	3.01	61.2	8.9	7.3	11.8
P18 (n=2)	3.27	57.2	10.4	7.7	13.2
P18 (n=3)	3.01	61.2	8.9	7.3	11.8
P19 (n=1)	3.07	53.3	17.9	3.6	16.8
P19 (n=2)	3.36	48.5	16.5	-0.7	11.3
P19 (n=3)	3.43	46.7	16.7	-2.9	8.7

Table S3 Continued

OSC	EA	BDE(AH⁻)	ΔG_{HYT}	ΔG_{ET}	ΔG_{H2}
P20 (n=1)	3.25	56.5	12.2	14.8	14.0
P20 (n=2)	3.51	53.1	9.7	12.0	8.8
P20 (n=3)	3.54	53.7	7.4	11.9	6.9
P21 (n=1)	2.98	69.6	5.0	15.1	20.8
P21 (n=2)	3.07	68.4	4.0	13.9	18.2
P21 (n=3)	3.15	67.5	5.2	13.3	18.4
P22 (n=1)	3.06	69.2	3.4	15.2	19.2
P22 (n=2)	3.22	67.0	1.8	12.4	14.3
P22 (n=3)	3.30	66.6	0.7	11.9	13.6
P23 (n=1)	3.56	60.5	1.2	7.0	7.5
P23 (n=2)	3.75	57.7	0.5	2.4	2.2
P23 (n=3)	3.76	58.6	-1.0	4.5	1.9
P24 (n=1)	3.59	55.3	4.5	0.3	4.4
P24 (n=2)	3.94	59.9	-8.1	4.3	-2.3
P24 (n=3)	4.03	57.2	-7.0	2.0	-4.1
P25 (n=1)	3.66	48.7	9.7	-7.6	4.2
P25 (n=2)	4.35	64.0	-20.9	-3.3	-11.1
P25 (n=3)	4.70	56.0	-20.8	-11.7	-19.5
P26 (n=1)	3.86	54.6	-1.7	11.0	-0.9
P26 (n=2)	4.29	57.1	-12.5	12.1	-11.3
P26 (n=3)	4.41	51.4	-10.0	5.0	-13.3
P27 (n=1)	3.60	50.0	9.3	1.1	5.0
P27 (n=2)	4.05	53.5	-4.1	-1.9	-5.7
P27 (n=3)	4.27	48.8	-4.2	-8.6	-12.7

Table S4. The EA of OSCs in eV and kinetic parameters in kcal/mol of HYT between *N*-DMBI-H and OSCs obtained at (U)M06-2X/6-311+G**// (U)B3LYP/6-31G** level with D3 correction in CHCl$_3$.

	EA	$\Delta H^{\ddagger}$ (298.15 K)	$\Delta G^{\ddagger}$ (298.15 K)	$\Delta H^{\ddagger}$ (373.15 K)	$\Delta G^{\ddagger}$ (373.15 K)
SM4	4.37	3.1	17.5	3.4	20.8
SM8	3.71	5.9	21.0	6.2	24.4
SM12	4.87	-6.7	9.1	-6.4	12.7
SM16	4.08	4.2	20.0	4.5	24.2
SM17	3.82	8.0	22.5	8.3	26.3
SM18	3.94	7.6	23.7	7.9	27.3
SM19	4.28	0.0	13.8	0.3	17.4
SM20	3.76	8.4	20.2	8.8	20.3
SM21	3.96	-5.6	11.0	-5.3	15.3
SM22	4.02	-7.1	10.9	-6.8	15.6
SM23	4.32	-9.5	7.8	-9.2	12.3
SM24	3.96	-0.2	17.1	0.1	21.6
SM25	4.72	-3.3	11.2	-3.0	14.5
P1 (n=1)	3.68	9.4	27.3	9.8	31.9
P2 (n=1)	3.46	5.7	21.1	6.0	25.1
P3 (n=1)	3.89	-5.2	11.8	-4.9	16.2
P4 (n=1)	4.03	-6.4	10.4	-6.1	14.8
P5 (n=1)	4.04	-7.3	10.1	-7.0	14.6
P6 (n=1)	3.74	-0.9	15.1	-0.6	19.3
P9 (n=1)	3.91	-7.4	11.1	-7.1	15.8
P11 (n=1)	2.60	21.1	36.5	22.0	40.9
P14 (n=1)	2.83	20.0	35.0	20.2	39.8
P15 (n=1)	3.41	10.4	24.7	10.7	28.4
P18 (n=1)	3.01	6.2	22.6	6.5	26.8
P20 (n=1)	3.25	11.9	27.8	12.2	32.0
P21 (n=1)	2.98	7.2	23.3	7.4	27.5
P23 (n=1)	3.56	-0.5	15.8	-0.2	20.0

References

1. A. E. Reed, R. B. Weinstock and F. Weinhold, *J. Chem. Phys.*, 1985, **83**, 735-746.
2. D. H. Ess and K. N. Houk, *J. Am. Chem. Soc.*, 2007, **129**, 10646-10647.
3. C. Li, D. Danovich and S. Shaik, *Chem. Sci.*, 2012, **3**, 1903-1918.
4. D. Usharani, D. C. Lacy, A. S. Borovik and S. Shaik, *J. Am. Chem. Soc.*, 2013, **135**, 17090-17104.
5. E. R. Johnson, S. Keinan, P. Mori-Sánchez, J. Contreras-García, A. J. Cohen and W. Yang, *J. Am. Chem. Soc.*, 2010, **132**, 6498-6506.
6. T. Lu and F. Chen, *J. Comput. Chem.*, 2012, **33**, 580-592.
7. R. A. Marcus, *Rev. Mod. Phys.*, 1993, **65**, 599-610.
8. G. S. Vadehra, R. P. Maloney, M. A. Garcia-Garibay and B. Dunn, *Chem. Mater.*, 2014, **26**, 7151-7157.
9. X. Zhan, A. Facchetti, S. Barlow, T. J. Marks, M. A. Ratner, M. R. Wasielewski and S. R. Marder, *Adv. Mater.*, 2011, **23**, 268-284.
10. K. L. Mutolo, E. I. Mayo, B. P. Rand, S. R. Forrest and M. E. Thompson, *J. Am. Chem. Soc.*, 2006, **128**, 8108-8109.
11. J.-H. Dou, Y.-Q. Zheng, Z.-F. Yao, Z.-A. Yu, T. Lei, X. Shen, X.-Y. Luo, J. Sun, S.-D. Zhang, Y.-F. Ding, G. Han, Y. Yi, J.-Y. Wang and J. Pei, *J. Am. Chem. Soc.*, 2015, **137**, 15947-15956.
12. T. Lei, J.-H. Dou, X.-Y. Cao, J.-Y. Wang and J. Pei, *J. Am. Chem. Soc.*, 2013, **135**, 12168-12171.
13. S. Fabiano, H. Yoshida, Z. Chen, A. Facchetti and M. A. Loi, *ACS Appl. Mater. Interfaces*, 2013, **5**, 4417-4422.
14. S. Wang, H. Sun, U. Ail, M. Vagin, P. O. A. Persson, J. W. Andreasen, W. Thiel, M. Berggren, X. Crispin, D. Fazzi and S. Fabiano, *Adv. Mater.*, 2016, **28**, 10764-10771.
15. J.-H. Dou, Y.-Q. Zheng, T. Lei, S.-D. Zhang, Z. Wang, W.-B. Zhang, J.-Y. Wang and J. Pei, *Adv. Funct. Mater.*, 2014, **24**, 6270-6278.
16. T. Lei, X. Xia, J.-Y. Wang, C.-J. Liu and J. Pei, *J. Am. Chem. Soc.*, 2014, **136**, 2135-2141.
17. K. Shi, F. Zhang, C.-A. Di, T.-W. Yan, Y. Zou, X. Zhou, D. Zhu, J.-Y. Wang and J. Pei, *J. Am. Chem. Soc.*, 2015, **137**, 6979-6982.
18. Y. Lu, Z.-D. Yu, H.-I. Un, Z.-F. Yao, H.-Y. You, W. Jin, L. Li, Z.-Y. Wang, B.-W. Dong, S. Barlow, E. Longhi, C.-a. Di, D. Zhu, J.-Y. Wang, C. Silva, S. R. Marder and J. Pei, *Adv. Mater.*, 2021, **33**, 2005946.
19. Y. Lu, Z. D. Yu, R. Z. Zhang, Z. F. Yao, H. Y. You, L. Jiang, H. I. Un, B. W. Dong, M. Xiong, J. Y. Wang and J. Pei, *Angew. Chem. Int. Ed.*, 2019, **58**, 11390-11394.
20. A. Onwubiko, W. Yue, C. Jellett, M. Xiao, H.-Y. Chen, M. K. Ravva, D. A. Hanifi, A.-C. Knall, B. Purushothaman, M. Nikolka, J.-C. Flores, A. Salleo, J.-L. Bredas, H. Sirringhaus, P. Hayoz and I. McCulloch, *Nat. Commun.*, 2018, **9**, 416.
21. Y. Shi, H. Guo, J. Huang, X. Zhang, Z. Wu, K. Yang, Y. Zhang, K. Feng, H. Y. Woo, R. P. Ortiz, M. Zhou and X. Guo, *Angew. Chem. Int. Ed.*, 2020, **59**, 14449-14457.
22. Y. Wang, H. Guo, A. Harbuzaru, M. A. Uddin, I. Arrechea-Marcos, S. Ling, J. Yu, Y. Tang, H. Sun, J. T. López Navarrete, R. P. Ortiz, H. Y. Woo and X. Guo, *J. Am. Chem. Soc.*, 2018, **140**, 6095-6108.
23. Y. Shi, H. Guo, M. Qin, Y. Wang, J. Zhao, H. Sun, H. Wang, Y. Wang, X. Zhou, A. Facchetti, X. Lu, M. Zhou and X. Guo, *Chem. Mater.*, 2018, **30**, 7988-8001.

24.   C. J. Mueller, C. R. Singh, M. Fried, S. Huettner and M. Thelakkat, *Adv. Funct. Mater.*, 2015, **25**, 2725-2736.

25.   X. Yan, M. Xiong, J.-T. Li, S. Zhang, Z. Ahmad, Y. Lu, Z.-Y. Wang, Z.-F. Yao, J.-Y. Wang, X. Gu and T. Lei, *J. Am. Chem. Soc.*, 2019, **141**, 20215-20221.